

Growth mechanism and origin of high sp^3 content in tetrahedral amorphous carbon

Miguel A. Caro,^{1,2,*} Volker L. Deringer,^{3,4} Jari Koskinen,⁵ Tomi Laurila,¹ and Gábor Csányi³

¹Department of Electrical Engineering and Automation, Aalto University, Espoo, Finland

²Department of Applied Physics, Aalto University, Espoo, Finland

³Engineering Laboratory, University of Cambridge,
Trumpington Street, Cambridge CB2 1PZ, United Kingdom

⁴Department of Chemistry, University of Cambridge,
Lensfield Road, Cambridge CB2 1EW, United Kingdom

⁵Department of Chemistry and Materials Science, Aalto University, Espoo, Finland

(Dated: September 26, 2018)

We study the deposition of tetrahedral amorphous carbon (ta-C) films from molecular dynamics simulations based on a machine-learned interatomic potential trained from density-functional theory data. For the first time, the high sp^3 fractions in excess of 85% observed experimentally have been reproduced by means of computational simulation and the deposition energy-dependence of the film's characteristics is also accurately described. High confidence in the potential and direct access to the atomic interactions allow us to infer the microscopic growth mechanism in this material. While the widespread view is that ta-C grows by "subplantation", we show that the so-called "peening" model is actually the dominant mechanism responsible for the high sp^3 content. We show that pressure waves lead to bond rearrangement away from the impact site of the incident ion, and high sp^3 fractions arise from a delicate balance of transitions between 3- and 4-fold coordinated carbon atoms. These results open the door for a microscopic understanding of carbon nanostructure formation with an unprecedented level of predictive power.

Amorphous carbons (a-C) are a class of materials with important applications as coatings. Of special interest are high-density forms of a-C which exhibit a high fraction of sp^3 -bonded carbon atoms, known as tetrahedral a-C (ta-C) or diamond-like carbon (DLC) because their mechanical properties are similar to those of diamond. Emerging applications of a-C are as precursors in the synthesis of other forms of nanostructured carbons [1, 2] and as a substrate platform for biocompatible electrochemical devices [3]. Significant efforts are being made to develop carbon-based devices designed for biological sensing, which could be implantable in the human body, and will be at the heart of the next technological revolution, where seamless integration between human tissue and microelectronics will enable real-time health monitoring and countless other applications [3–5].

Together with its widespread technological and industrial use, a-C has also been the subject of significant academic interest, in particular by the computational modeling community. The high degree of bonding flexibility exhibited by carbon, which can exist in sp^3 , sp^2 and sp environments or "hybridizations", is behind its ability to form numerous compounds which make the sheer complexity of life possible. This flexibility is also responsible for the large degree of microscopic variability found in a-C, where diverse and disordered atomic motifs can coexist, each in its own metastable configuration. This makes simulations of a-C a long-standing challenge for any computational model based on interatomic potentials. Early molecular dynamics (MD) studies focused on optimizing and parameterizing simple classical potentials for a-C [6], but also seminal *ab initio* MD (AIMD) simulations of a-C were conducted when the field was still in

its infancy [7, 8]. A constant struggle for computational models, since early on and until today, has been to recreate and understand the formation process which leads to the high sp^3 fractions observed for ta-C, which can be in excess of 85%. Experimentally, ta-C is commonly grown by deposition of energetic ions onto a substrate. The fraction of sp^3 carbon increases monotonically with the beam energy up to approximately 60 eV–100 eV (depending on the method) [9], where it peaks at around 90%. At higher energies, the amount of sp^3 atoms starts to diminish. Unfortunately, this is an extremely challenging process to study using highly accurate methods, such as AIMD based on density-functional theory (DFT), due to their computational cost. Instead, simulated deposition has been carried out in the past with "classical" interatomic potentials such as Tersoff [6] and C-EDIP [10]. However, classical potentials have systematically failed at reproducing experimentally observed sp^3 fractions [11]. DFT-based generation of a-C has been carried out with varying degree of success using alternative routes [12–14]. See Ref. [3] for a review of the performance of different generation methods and potentials.

Thus, there is a gap between what would be a close representation of reality and what can be simulated in practice. This gap is due to the difficulty of modeling realistic processes (large number of atoms, long time scales) and what can currently be done with accurate, yet computationally-expensive methods, such as DFT-based MD. Recent advances in computational techniques have given rise to a trend in the physics, chemistry and materials science communities to apply machine-learning (ML) and data-driven approaches to materials modeling [16, 17]. In the specific realm of interatomic po-

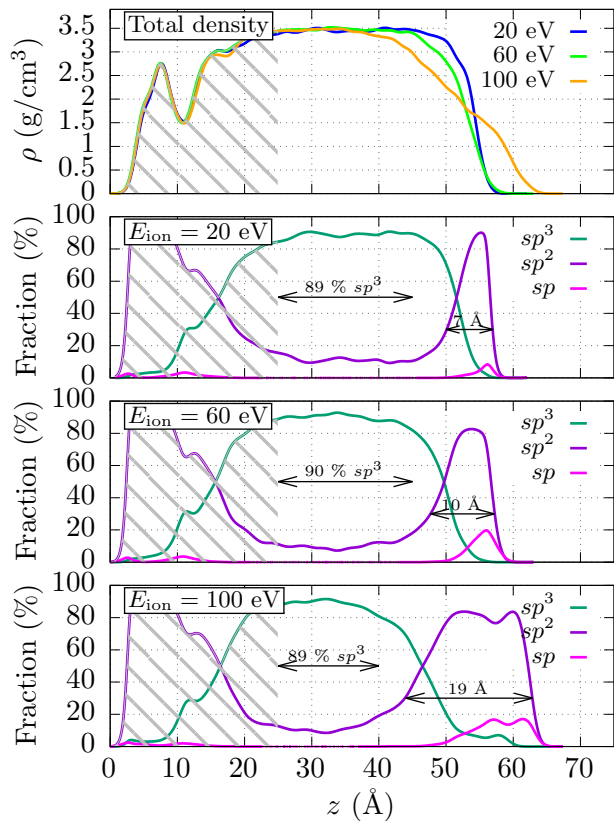


FIG. 1. Mass density profiles and sp , sp^2 and sp^3 fractions in the bulk of the film, for the different deposition regimes studied. Atomic coordinations are determined according to a 1.9 Å cutoff radius for nearest neighbors, which corresponds to the first minimum of the radial distribution function [15].

entials, a family of general and highly flexible potentials referred to as “Gaussian approximation potentials” (GAPs) has been introduced, which promises to bridge the gap we were referring to earlier [18]. In this Letter, we use the GAP ML interatomic potential [19] to study the hitherto unresolved a-C growth mechanism and the physical reasons for the high sp^3 concentration in ta-C films with an unprecedented level of accuracy.

To study the atomistic details of the growth of an a-C film, we explicitly simulated the deposition of C atoms onto a carbon substrate *one atom at a time*, using MD. A large [111]-oriented diamond substrate, terminated by the stable 2×1 surface reconstruction, was used, containing 3240 atoms in periodic boundary conditions. This corresponds to initial dimensions of $38 \text{ \AA} \times 38 \text{ \AA}$ in plane and 16 \AA of thickness. The effect of the substrate on the results of the simulation is discussed in the Supplemental Information (SI). 2500 single monoenergetic C atoms with a kinetic energy of 60 eV were dropped from the top of the simulation box onto the diamond substrate, to create an initial a-C template. After this, an additional 5500 atoms, each with a kinetic energy corresponding to the different deposition regimes studied (20 eV, 60 eV

and 100 eV), were subsequently deposited, for a total of 8000 impact events per energy. The equations of motion were integrated using a time step dynamically adapted to correctly describe the atomic trajectories while maximizing computing efficiency, ensuring that the largest atomic displacements do not exceed 0.1 Å per time step. Our main results are obtained with the GAP ML potential trained from local density approximation (LDA) DFT data [19]. All MD simulations were carried out with LAMMPS [20, 21].

The impact of the incident ions *per se* lasts for just a few fs. However, the kinetic energy of the impacting atom is transferred to the substrate, increasing its temperature. To ensure that the experimental conditions are met as closely as possible, this extra kinetic energy needs to be removed using a thermostat, bringing the system back to equilibrium before the next deposition takes place. Equilibrating the system back to the nominal substrate temperature, 300 K, takes up to 1 ps, depending on the energy of the incident ion. Equilibration is therefore by far the most computationally expensive part of the simulation. A more detailed discussion of the dependence on deposition energy (including the low-energy regime), an in-depth study of elasticity and comparison with Tersoff and C-EDIP results will be published later in a more technical paper [22]. Video animations of the growth process can be accessed online from the Zenodo repository [23] and the SI.

In Fig. 1 we show the main structural features of the deposited a-C films. The figure shows the in-plane averaged mass density profile of the films grown at different deposition energies. Very high densities and sp^3 fractions are obtained in the interior of the film. The simulated deposition at 60 eV, which is the ion energy at which sp^3 content is expected to peak based on experimental observations [24], shows sp^3 fractions of up to 90%. Previous simulations [3, 11, 13, 15], either based on deposition or alternative methods such as liquid quenching, have systematically failed to reproduce these high numbers. The previously reported computational results with the highest sp^3 fractions (shy of 85%) were based on DFT geometry optimization followed by pressure correction [3, 15]. Explicit deposition simulations (based on the widely used empirical C-EDIP potential) had not been able to produce a-C structures with sp^3 fractions exceeding $\sim 60\%$ [11]. The 20 eV, 60 eV and 100 eV films from Fig. 1 reach mass densities around 3.5 g/cm^3 , very close to diamond. Although these densities exceed typical experimental values for ta-C by a few percent, is it indeed possible to grow “superhard” ta-C close to the density of diamond under ideal conditions, such as the absence of hydrogen [25]. Lifshitz *et al.* showed that ta-C films as dense as 3.5 g/cm^3 can be grown consistently over a wide range of deposition energies [26], although we must note that such extremely high-density samples are lacking from most of the literature, where quoted values

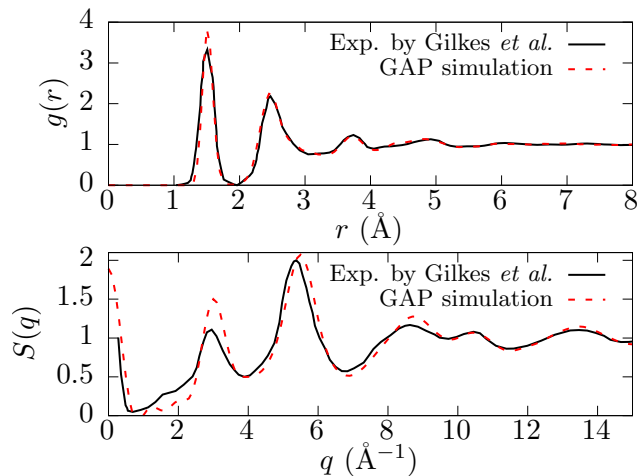


FIG. 2. Radial distribution function and structure factor in the bulk region of the film, extracted from the 60 eV deposition simulations, and comparison with experimental data from Gilkes *et al.* [27].

are typically below the 3.3 g/cm³ mark. One also needs to take into consideration that these ta-C films are under typical compressive stresses equivalent to $\sim 2\%$ change in volume (Table I).

The comparison with experimental fingerprints for short and medium range order (Fig. 2) again reveals excellent agreement and further indicates that GAP provides a correct description of the deposition physics. The elastic properties of the films, including stresses built-in during deposition, are summarized in Table I. We note that GAP has previously been tested to give reliable elastic properties for quenched a-C [19]. For the present study, we computed the elastic properties of the films in the bulk-like region, that is, the portion of the film where the sp^3 fraction remains constant. Details will be given in a separate paper, which also presents more detailed information on the elastic properties of the films and their energy dependence [22]. The data in Table I indeed confirm that ta-C films are under large compressive stresses, of the order of 10 GPa. Under such compression, this superhard ta-C film is less compressible than diamond at equilibrium, for which the bulk modulus is ~ 440 GPa. The elastic moduli should be significantly reduced once the strain in the film is released. We observed plastic deformation (bond rearrangement) when attempting film relaxation. Based on this and on abundant experimental evidence [9], it is unlikely that highly sp^3 -rich ta-C can be generated in the absence of these large compressive stresses. What is more difficult to ascertain is whether compressive stress is required for ta-C growth or just a consequence of how growth occurs.

With regards to surface morphology, Fig. 1 already clearly hints toward different features as the deposition energy is varied. As the ion energy increases, the spatial extent of the sp^2 -rich region increases too. This can be

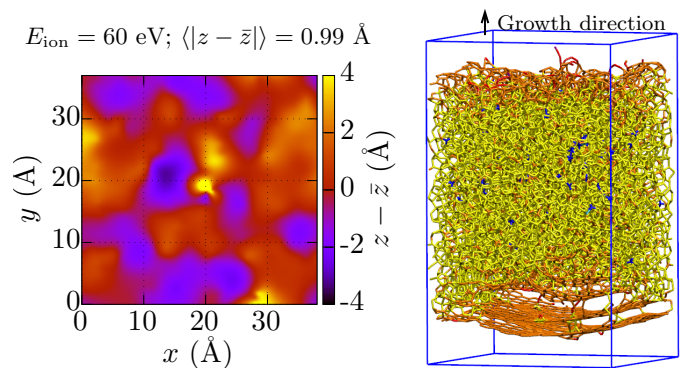


FIG. 3. Surface roughness and atomic film structure of the 60 eV system, calculated as the mean absolute deviation of surface height from its average. Purple, red, orange, yellow and blue atoms represent 1-, 2-, 3-, 4- and 5-fold coordinated C atoms, respectively. The reason for graphitization of the lower surface and the presence of a few 5-fold coordinated C atoms are discussed in the SI.

observed in more detail in Fig. 3, where we show the final deposited film structure for 60 eV and its topographic surface map. The microscopic surface roughness for this film is ~ 1 Å. We observe that surface roughness is minimal for the 20 eV film (~ 0.7 Å), and increases for both lower and higher deposition energies (e.g., ~ 1.5 Å and ~ 1.9 Å at 5 eV and 100 eV, respectively) [22]. These results are in qualitative agreement with the detailed experimental study on the morphology of ta-C surfaces by Davis *et al.* [29], who measured ~ 4 Å and ~ 10 Å thick sp^2 -rich regions for 35 eV and 100 eV films, respectively. Although Davis’ data for surface thickness have large error bars, and the definition of a “surface region” is to some degree arbitrary, we can infer that surface thickness increases experimentally between 0.1 Å/eV and 0.2 Å/eV within the energy regime relevant to ta-C growth [29]. In

TABLE I. Elastic properties of the as-grown film (60 eV deposition).

Quantity	Simulation	Experiment
In-plane stress ($\frac{\sigma_1 + \sigma_2}{2}$)	-14.4 GPa	
Out-of-plane stress (σ_3)	0 GPa	
Stress (isotropic average)	-9.6 GPa	-10 GPa ^a
Equivalent in-plane strain	-1.4 %	
Equivalent out-of-plane strain	0.8 %	
Bulk modulus	547 GPa	397 GPa ^a
Young’s modulus	810 GPa	760 ^a , 850 ^b GPa

^a Ferrari *et al.* [28] for a 3.26 g/cm³ sample. Although the authors report 340 GPa as bulk modulus, we note that 397 GPa is the value which best fits their data when considering the full domain of elastic moduli compatible with the experimental measurements [22].

^b Schultrich *et al.* [25] for a 3.43 g/cm³ sample.

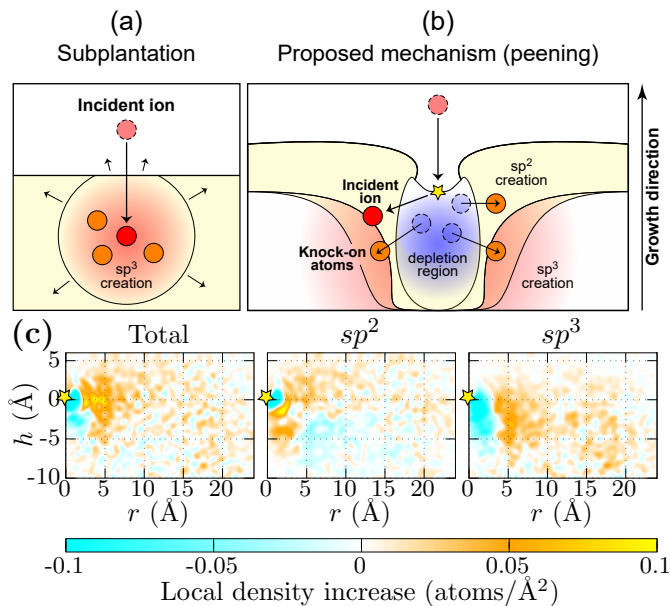


FIG. 4. (a) Previously accepted growth mechanism in t-C and (b) growth mechanism proposed in this Letter. (c) Average increase in local mass density after ion impact (60 eV deposition, see text for details). The star indicates the impact site.

this context, our estimates of surface thickness (Fig. 1) also show reasonable quantitative agreement with experiment. The general conclusion is that the thickness of the surface region grows with deposition energy, due to the increasing strength of the local thermal spike at the impact site. Impacting atoms induce generation of sp^2 -bonded carbon, including *local* transition from sp^3 to sp^2 coordination.

We now turn our attention to the microscopic growth mechanism responsible for these high sp^3 fractions. The consensus in the literature is that the “subplantation” mechanism is behind this phenomenon [24]. This mechanism is illustrated in Fig. 4 and relates the increase in bonding coordination to the packing of atoms in too small a volume, as newly arrived atoms are being deposited. The relaxation of the surrounding matrix then explains film growth. However, this view is in contradiction with the results of our simulations. While the subplantation mechanism was already challenged by Marks from C-EDIP simulations [11], one of the reasons why an alternative model as already proposed with C-EDIP has not been accepted is the lack of quantitative agreement with experiment, i.e., the sp^3 fractions are too low as predicted by C-EDIP. In Fig. 4 (c) we show the local mass density difference between the structure before and after impact:

$$\Delta\rho(r, h) = 2\pi r (g_{\text{after}}(r, h) - g_{\text{before}}(r, h)), \quad (1)$$

where $g(r, h)$ is the pair correlation function on the surface of a cylinder of radius r and height h with origin at

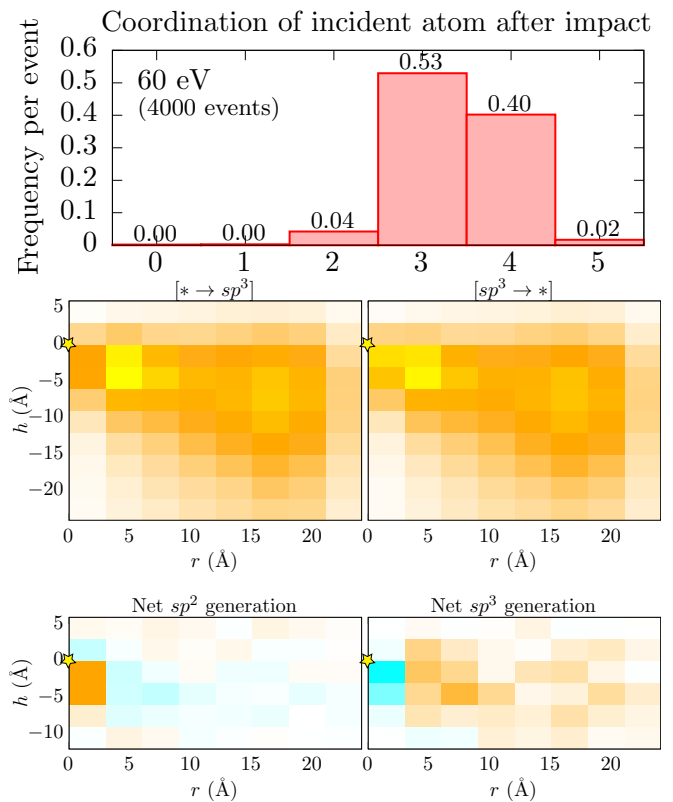


FIG. 5. (Top) Distribution of coordinations for the incident atom after deposition. (Middle) Average bond rearrangements that take place for each impact, from and to sp^3 coordination, as a function of depth and lateral distance from impact site. (Bottom) Net generation of sp^3 sites and sp^2 sites (both excluding incident atom contribution). Blue, orange and yellow indicate negative, positive and very positive bond rearrangement, respectively. The star indicates the impact site. An enlarged version of the middle and bottom panels of this figure, with additional quantitative information, is given in the SI.

the impact site. $\Delta\rho(r, h)$ therefore gives the difference in total atom density integrated on a circumference of radius r around the impact site at height h . We furthermore resolve this according to sp^2 and sp^3 components, which are computed with Eq. (1) using only the partial local mass densities corresponding to atoms with 3- and 4-fold coordination, respectively. This quantity allows us to visualize where atoms are being removed and deposited and where the transition from sp^2 to sp^3 is taking place. Orange regions in the color maps indicate an increase in local density after impact, whereas blue regions denote a decrease in local density. The origin of the plot, $(0,0)$, corresponds to the impact site, and the maps have been averaged over the last 4000 impacts. Our results challenge the belief that subplantation explains the high sp^3 fractions. The blue region around and below the impact site on the “Total” and “ sp^3 ” panels shows that atoms are being displaced by the incoming ion. The orange region circling the impact site in the “ sp^2 ” panel

shows that these atoms, including the incoming ion, are subsequently deposited preferentially as sp^2 atoms.

To further quantify this effect, Fig. 5 shows the average changes in atomic coordination within different regions around the impact site. As mentioned, the impacting atom is preferentially deposited with 3-fold coordination and there is a net *annihilation* of 4-fold (sp^3) sites in the immediate vicinity of the impact site. This is incompatible with the subplantation mechanism, which would require a majority of impacting atoms to be deposited with 4-fold coordination (see SI for more quantitative information). Our data show that each single impact induces coordination changes for roughly 80 atoms, and that sp^3 motifs locally diminish at and around the impact site. However, the dynamical balance between sp^3 creation and annihilation builds up *laterally and away* from the impact region to yield net generation of sp^3 carbon as a result. Figure 4 (b) shows schematically how the atoms are locally depleted around the impact site and deposited nearby as sp^2 carbon. This displacement induces a transformation of the surrounding carbons from sp^2 to sp^3 , and also the film's growth via vertical displacement of the uppermost layer of C atoms, which are always predominantly sp^2 -bonded (and occasionally sp). Therefore, our results indicate that the pressure wave generated by the impacting energetic ions and knock-on atoms is responsible for the generation of sp^3 -rich a-C films. This process is beneficial at the studied 20 eV, 60 eV and 100 eV deposition energies, but it does not occur at lower energies [22]. As the deposition energy increases, the incoming ions carry enough kinetic energy to start damaging the surface, which leads to the creation of a thicker and more disordered sp^2 surface region (Figs. 1 and 3), in agreement with experiment [29].

To summarize, this is the first computational study to report deposited a-C structures with a degree of sp^3 hybridization in quantitative agreement with experiment. Most importantly, the excellent agreement that we obtain with relevant experiments gives us confidence that our simulation is reproducing the microscopic physical processes correctly. In turn, this gives us confidence that we provide a fully atomistic account of the growth mechanism and high sp^3 contents in ta-C. The growth mechanism clearly supported by our results is peening; the previously proposed subplantation mechanism cannot be substantiated in view of our data. The use of a machine-learned interatomic potential trained from *ab initio* data has allowed us to achieve a level of description for this complex problem that has previously been out of reach. We believe these results also highlight the role that machine learning will play in the field of materials modeling and molecular dynamics in the years to come.

This research was financially supported by the Academy of Finland through grants 310574 and 285526. Computational resources were provided by CSC – IT Center for Science, Finland, through projects 2000634 and

2000300. V. L. D. gratefully acknowledges a fellowship from the Alexander von Humboldt Foundation, a Leverhulme Early Career Fellowship, and support from the Isaac Newton Trust.

* mcaroba@gmail.com

- [1] S. Sainio, H. Jiang, M. A. Caro, J. Koehne, O. Lopez-Acevedo, J. Koskinen, M. Meyyappan, and T. Laurila, “Structural morphology of carbon nanofibers grown on different substrates,” *Carbon* **98**, 343 (2016).
- [2] I. Suarez-Martinez and N. A. Marks, “Amorphous carbon nanorods as a precursor for carbon nanotubes,” *Carbon* **50**, 5441 (2012).
- [3] T. Laurila, S. Sainio, and M. A. Caro, “Hybrid carbon based nanomaterials for electrochemical detection of biomolecules,” *Prog. Mater. Sci.* **88**, 499 (2017).
- [4] J. N. Tiwari, V. Vij, K. C. Kemp, and K. S. Kim, “Engineered carbon-nanomaterial-based electrochemical sensors for biomolecules,” *ACS nano* **10**, 46 (2015).
- [5] R. I. Arriaga, M. Findlay, P. J. Hesketh, and J. R. Stetter, “Ubiquitous wearable electrochemical sensors,” *Electrochem. Soc. Interface* **25**, 69 (2016).
- [6] J. Tersoff, “Empirical interatomic potential for carbon, with applications to amorphous carbon,” *Phys. Rev. Lett.* **61**, 2879 (1988).
- [7] G. Galli, R. M. Martin, R. Car, and M. Parrinello, “Structural and electronic properties of amorphous carbon,” *Phys. Rev. Lett.* **62**, 555 (1989).
- [8] H.-P. Kaukonen and R. M. Nieminen, “Molecular-dynamics simulation of the growth of diamondlike films by energetic carbon-atom beams,” *Phys. Rev. Lett.* **68**, 620 (1992).
- [9] J. Robertson, “Diamond-like amorphous carbon,” *Mat. Sci. Eng. R* **37**, 129 (2002).
- [10] N. A. Marks, “Generalizing the environment-dependent interaction potential for carbon,” *Phys. Rev. B* **63**, 035401 (2000).
- [11] N. A. Marks, “Thin film deposition of tetrahedral amorphous carbon: a molecular dynamics study,” *Diam. Relat. Mater.* **14**, 1223 (2005).
- [12] N. A. Marks, D. R. McKenzie, B. A. Pailthorpe, M. Bernasconi, and M. Parrinello, “*Ab initio* simulations of tetrahedral amorphous carbon,” *Phys. Rev. B* **54**, 9703 (1996).
- [13] D. G. McCulloch, D. R. McKenzie, and C. M. Goringe, “*Ab initio* simulations of the structure of amorphous carbon,” *Phys. Rev. B* **61**, 2349 (2000).
- [14] N. A. Marks, N. C. Cooper, D. R. McKenzie, D. G. McCulloch, P. Bath, and S. P. Russo, “Comparison of density-functional, tight-binding, and empirical methods for the simulation of amorphous carbon,” *Phys. Rev. B* **65**, 075411 (2002).
- [15] M. A. Caro, R. Zoubkoff, O. Lopez-Acevedo, and T. Laurila, “Atomic and electronic structure of tetrahedral amorphous carbon surfaces from density functional theory: Properties and simulation strategies,” *Carbon* **77**, 1168 (2014).
- [16] R. Z. Khaliullin, H. Eshet, T. D. Kühne, J. Behler, and M. Parrinello, “Nucleation mechanism for the direct graphite-to-diamond phase transition,” *Nature materials*

- 10, 693 (2011).
- [17] G. C. Sosso, G. Miceli, S. Caravati, F. Giberti, J. Behler, and M. Bernasconi, “Fast crystallization of the phase change compound GeTe by large-scale molecular dynamics simulations,” *J. Phys. Chem. Lett.* **4**, 4241 (2013).
- [18] A. P. Bartók, M. C. Payne, R. Kondor, and G. Csányi, “Gaussian approximation potentials: The accuracy of quantum mechanics, without the electrons,” *Phys. Rev. Lett.* **104**, 136403 (2010).
- [19] V. L. Deringer and G. Csányi, “Machine learning based interatomic potential for amorphous carbon,” *Phys. Rev. B* **95**, 094203 (2017).
- [20] S. Plimpton, “Fast parallel algorithms for short-range molecular dynamics,” *J. Comput. Phys.* **117**, 1 (1995).
- [21] <http://lammmps.sandia.gov>.
- [22] M. A. Caro, V. L. Deringer, J. Koskinen, T. Laurila, and G. Csányi, “Machine-learning-based simulated deposition of sp^3 -rich amorphous carbon films,” in preparation (2018).
- [23] M. A. Caro, “Deposition of amorphous carbon at different energies modeled with GAP,” Zenodo (2017), DOI:10.5281/zenodo.1133425.
- [24] J. Robertson, “Plasma deposition of diamond-like carbon,” *Jpn. J. Appl. Phys.* **50**, 01AF01 (2011).
- [25] B. Schultrich, H.-J. Scheibe, D. Drescher, and H. Ziegele, “Deposition of superhard amorphous carbon films by pulsed vacuum arc deposition,” *Surf. Coat. Tech.* **98**, 1097 (1998).
- [26] Y. Lifshitz, G. D. Lempert, E. Grossman, I. Avigal, C. Uzan-Saguy, R. Kalish, J. Kulik, D. Marton, and J. W. Rabalais, “Growth mechanisms of DLC films from C^+ ions: experimental studies,” *Diam. Relat. Mater.* **4**, 318 (1995).
- [27] K. W. R. Gilkes, P. H. Gaskell, and J. Robertson, “Comparison of neutron-scattering data for tetrahedral amorphous carbon with structural models,” *Phys. Rev. B* **51**, 12303 (1995).
- [28] A. C. Ferrari, J. Robertson, M. G. Beghi, C. E. Bottani, R. Ferulano, and R. Pastorelli, “Elastic constants of tetrahedral amorphous carbon films by surface Brillouin scattering,” *Appl. Phys. Lett.* **75**, 1893 (1999).
- [29] C. A. Davis, G. A. J. Amaratunga, and K. M. Knowles, “Growth mechanism and cross-sectional structure of tetrahedral amorphous carbon thin films,” *Phys. Rev. Lett.* **80**, 3280 (1998).